第31卷第6期
2012年12月

红外与毫米波学报
J. Infrared Millim. Waves

Vol. 31, No. 6
December, 2012

文章编号:1001-9014(2012)06-0481-06

DOI:10.3724/SP.J.1010.2012.00481

Peak detection wavelength at 8 μm: accurate design and fabrication of quantum well infrared photodetector

JIN Ju-Peng, LIU Dan, CHEN Jian-Xin, LIN Chun

(Key Laboratory of Infrared Imaging Materials and Detectors, Shanghai Institute of Technical Physics, Chinese Academy of Sciences, Shanghai 200083, China)

Abstract: Using one band effective mass approximation and shooting method, optimized parameters of quantum well infrared photodetector structure were calculated. Taking into account high order effect of band nonparabolicity, the device structure with a peak detection wavelength of 8 μm were designed. Based on the calculated result, GaAs/AlGaAs multiwell material was grown. Then single-element QWIP device were fabricated and characterized. Symmetrical *I-V* curves showed very good quality of the material and successful process in device fabrication. Spectral responsivity exhibited peak wavelength of 7.96 and 7.98 μm, which were in excellent agreement with our designed value.

Key words: QWIP; GaAs/AlGaAs; peak detection wavelength; spectral responsivity; band nonparabolicity

PACS: 78.67.De, 78.55.Cr, 78.30.Fs

量子阱红外探测器峰值探测波长的精确设计与实验验证

金巨鹏, 刘 丹, 陈建新, 林春

(中国科学院上海技术物理研究所 红外成像材料与器件重点实验室,上海 200083)

摘要:采用单能带电子有效质量近似(EMA)和波包函数近似(EFA)模型,考虑了能带非抛物线性等高阶因素,并利用投试法求解薛定谔方程,计算了准确设计峰值探测波长的GaAs/AlGaAs量子阱探测器结构参数.基于计算结果,用分子束外延(MBE)方法生长了设计峰值波长为8 μm的GaAs/AlGaAs多量子阱材料,进而制备了单元器件,并测试了*I-V*曲线、光谱响应和探测率.*I-V*曲线的良好对称性显示了材料生长与器件制备工艺的质量,光谱响应曲线表明器件实际的峰值探测波长为7.96 ~7.98 μm,与设计预期值吻合.

关 键 词:量子阱红外探测器;GaAs/AlGaAs;峰值波长;光谱响应;能带非抛物线性

中图分类号:O472+.3, O471.5 **文献标识码**:A

Introduction

Quantum well infrared photodetectors (QWIP) have been a very important research topic in infrared detector area for more than 20 years. Since the first observation of strong infrared intersubband absorption in GaAs/AlAs quantum-well wave-guides structure[1] in 1987, QWIP have rapidly progressed and became relatively mature. Compared with the traditional dominant HgCdTe (mercury cadmium telluride, MCT) detector[2], QWIP have the advantages of good uniformity, multiband detect capacity, much lower cost, and relatively mature process[3]. Especially, in the long-wave infrared (LWIR) range, MCT detectors suffer from weak mechanical strength due to the weak bonding, low uniformity due to the high Hg vapor pressure, low yield and high cost due to the difficulty in production. Since large substrate is preferred in large format focal plane array (FPA) fabrication, the small size of CdZnTe substrate further increase the difficulty that MCT confronted[4]. This makes QWIP find its way for application in LWIR band and large scale FPA.

Received date: 2011-06-17, **revised date**: 2012-03-01 **收稿日期**:2011-03-19, **修回日期**:2012-03-01

Biography: JIN Ju-Peng(1982-), male, Lanzhou, China. Ph. D. Research fields focus on III-V compound of semiconductor devices. E-mail: jinjupeng@gmail.com.

QWIPs make use of intersubband transition to detect photons, while MCT photodetectors are based on interband transition in intrinsic variable gap semiconductor. Figure 1 schematically depicts this difference. Besides, QWIP is not sensitive to the incident light parallel to the growth direction.

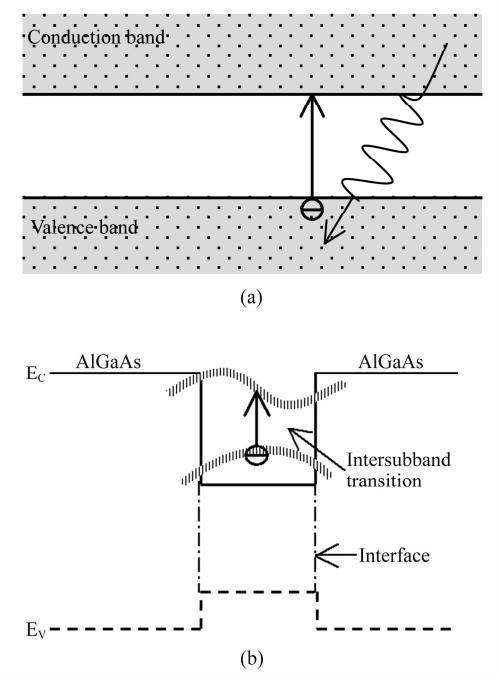

Fig. 1 Schematic picture exhibiting the different absorption mechanism of MCT and QWIP
图 1 镉镉汞探测器与量子阱红外探测器不同的红外吸收机理示意图

In this paper we report on the design and fabrication of QWIP for certain peak detection wavelength in LWIR. One band effective mass approximation (EMA) model and envelop function approximation (EFA) were employed in device design, and shooting method was chosen in concrete calculation. QWIP structure parameters with an objective peak detection wavelength of 8 μm were calculated. Based on the calculated result, multiwell QWIP devices were fabricated and characterized. All samples showed satisfactory detectivity and the experimental result of peak wavelength is in good agreement with our expected value.

1 Modeling and design

1.1 Basic model and computation method

We made use of EMA and EFA to find the quantized energy levels of electrons in the wells as well as their corresponding wave function. As the most widely used approximation method in semiconductor physics, EMA turns the complexity of crystal material potential into simplicity of an empirically fitted constant, i. e. effective mass. Effective mass varies for different semiconductor materials and can be experimentally determined. Under the modeling of EMA, the time-independent Schrödinger equation for an electron in bulk semiconductor can be written as

$$-\frac{\hbar^2}{2m^*}\frac{\partial^2}{\partial z^2}\psi(z) = E(z), \tag{1}$$

where m^*, $\hbar$, $\psi$and E are effective mass, Plank constant, wavefunction and eigenenergy value respectively. For heterostructure composed of two kinds of materials with different band gap, EFA is widely accepted and applied as a good approximation on materials. Holding the assumptions that EMA is still valid in each bulk material and the heterojunction can be described by one material potential which derives from the discrepancy in bandgaps, the Schrödinger equation describing the electron behavior in heterostructure can be written in the form:

$$-.\frac{\hbar^2}{2m^*}\frac{\partial^2}{\partial z^2}\psi(z) + V(z)\psi(z) = E\psi(z). \tag{2}$$

This manipulation is so-called EFA. The subsequent problem is solving the Schrödinger equation like Eq. 2.

Shooting method has been proved to be a very flexible and powerful approach to solve differential equation like Schrödinger equation. The principal idea of this approach is the approximation changing derivative into finite difference, i. e. replace $\frac{\mathrm{d}f}{\mathrm{d}z}$ by $\frac{\Delta f}{\Delta z}$.

Take $m^*(z)$ to be the mean value of $m^*(z+\delta z/2)$ and $m^*(z-\delta z/2)$, the iteration formula in shooting method is

$$\frac{\psi(z+\delta z)}{m^*(z+\delta z/2)} = \left\{\frac{2(\delta z)^2}{\hbar^2}[V(z)-E] + \frac{1}{m^*(z+\delta z/2)} + \frac{1}{m^*(z-\delta z/2)}\right\}\psi(z) - \frac{\psi(z-\delta z)}{m^*(z-\delta z/2)}$$

Knowing the values of two points, $\psi(z-\delta z)$ and $\psi(z)$, the third points $\psi(z+\delta z)$ can be calculated. Doing the same procedure iteratively, the whole wave function can be calculated for any specific energy value. The boundary condition for stationary state is

$\psi(z)\to 0$ and $\frac{\partial}{\partial z}\psi(z)\to 0$ when $z\to\pm\infty$. We can systematically change the value of energy stepwise and find out the value satisfy the boundary condition, which is the eigenenergy for a stationary state in QWs.

The model described above does not take into account any actual situation in device design. Higher order effects such as multi particle effect, quantum-confined Stark effect and band-nonparabolicity have considerable influence on the energy levels of quantum wells (QWs). Hence, these higher order effects should be considered in QWIP designing.

Practically, QWIPs are heavily doped in the well region and there are tremendous free electrons in wells, the important assumption of EMA model that there is one single electron in the potential filed is not valid any more. The multiple electrons doped in wells make the potential edge slightly changed. Self-consistent solution of Poisson and Schrodinger equation often employed to include this multi particle effect. The result shows an increase of the ground state level in wells for several meV[5], which lead to a red shift of the peak detection wavelength of a QWIP.

Since a conductive QWIP commonly work under certain bias voltage, the electrical field leads to quantum-confined Stark effect, which is known as the suppression of the ground state level in the wells. The effect is more significant under high bias. As a result, the ground levels in quantum wells decrease by a few meV[6]. This leads to a blue shift of the detection wavelength of a QWIP. The multi-particle effect and quantum confined Stark-effect has opposite influence on the ground state level in QWs, what is important, the influence of these two effects are comparable. Hence, these two effects may offset each other and can be eliminated from the detector modeling to simplify the computation. Finally, higher order effect of band nonparabolicity is included in our QWIP device design and cumbersome calculation was avoided.

The parabolic relation given by $E=\hbar^2k^2/2m^*$ is valid for the situation that the energy of the electron is very close to the band edge. When electron energy goes far away from band edge, the band nonparabolicity effect becomes non-negligible for its effect on dark current[7]. We took into account band nonparabolicity by the formula proposed by Y. Hirayama et. al since its simplicity to include into the shooting method calculation[8]. The effective mass parameter was expressed in the form of $m^*(E)=m_*(0)[1+\alpha(E-V)]$, where $\alpha=[1-m^*(0)/m_0]^2/E_g$, instead of the parabolic relation given by $E=\hbar^2k^2/2m^*$. Finally, we made the iteration computation including band nonparabolicity with MatLab.

1.2 Device design

As a general rule, Photoconductive QWIP will have a better performance when the first excited states of the well is resonant with the barrier height[9], and the energy difference between the excited state and ground state determines the peak detection wavelength. According to this rule, parameters such as well width and barrier height for a given peak absorption wavelength can be calculated.

We made a systematical calculation for GaAs/AlGaAs QWIP and the result is showed in Fig. 2, where the strong red line display that the optimum combination of well width and barrier height for detection wavelength from 7 to 16 μm.

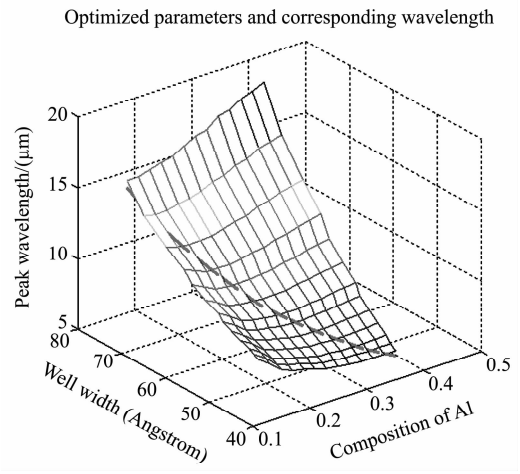

Fig. 2　Optimized combinations of well width and barrier for peak detection wavelength for 7 to 16μm
图 2　峰值探测波长从 7 到 16μm 的最佳阱宽与势垒的组合

We designed the parameters of a QWIP with an expected peak detection wavelength of 8 μm. The well width and Al fraction are calculated to be 5.2 nm and 0.28 respectively. The doping density in the well layer introduces another degree of freedom in design. As-

suming that the dopants in the wells are completely ionized, the relationship between Fermi energy level and the 2D doping density is $N_D = (m^* \pi \hbar^2) E_f$. We determined the doping level by $E_f = 2k_B T$. Here E_f is Fermi energy, k_B is Boltzman constant, and the doping density was calculated to be 6.0×10^{17} cm^{-3}. In addition, the thickness of the AlGaAs barrier layer also needs careful consideration. The barrier should be thick enough to suppress the interwell tunneling current and limit the dark current. And there exist a critical barrier width value, beyond which the dark current will not be reduced any more. This critical barrier thickness is in the range of 20 ~ 30 nm[10]. 30 nm were chosen as the barrier width. Figure 3 shows the designed structure details. The multiple quantum well regions have 20 and 40 periods of wells for two samples respectively. Table 1 indicates the concrete value we adopted for some material parameters in calculation[11].

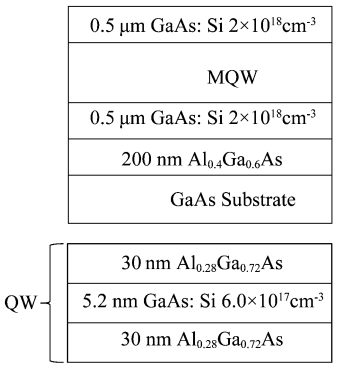

Fig. 3 The schematic diagram illustrating the designed well structure
图3 设计的量子阱结构示意图

Table 1 Arguments we adopted for GaAs and AlGaAs in shooting method
表1 投试法计算中采用的 GaAs 和 AlGaAs 的参数

	m^*	E_g
GaAs	$0.67\ m_0$	1.412 eV
$Al_xGa_{1-x}As$	$(0.067 + 0.083x)m_0$	$1.247 \times 0.67x$ eV

2 Devices fabrication

Based on the result of the calculation, corresponding GaAs/AlGaAs quantum well structure was grown by molecular beam epitaxy (MBE) on a 2 inches diameter GaAs substrate. Two samples with 20 and 40 wells were grown. Then Standard lithography process, wet etching, and thermal metallic evaporation process were employed in fabricating the device. A mixed solution of pure sulfuric acid, hydrogen peroxide, and water was used for wet etching. AuGeNi alloy was deposited on the top of the mesas and the bottom contact layer, and then annealed to form good ohmic contact. Finally a relatively thick pure Au layer of about 500 nm was deposited on top and bottom contact to provide sufficient mechanical strength for wire bonding. The finished single element device chips were then carefully polished to form a 45° facet at the GaAs substrate, which is used to couple the infrared radiance. Figure 4 shows the whole configuration.

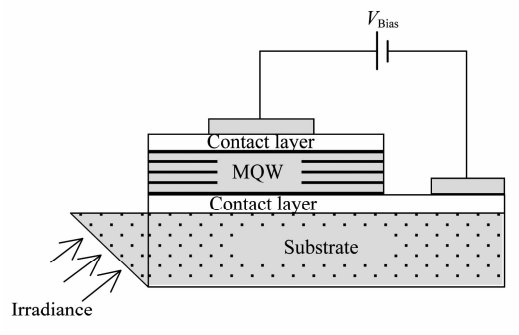

Fig. 4 Schematic profile diagram of the final device with 45° angle on GaAs substrate
图4 具有45°倒角的 GaAs 衬底器件剖面示意图

3 Experimental result

After the sample devices were completely processed, two sample devices, sample 1 with 20 repeats in MQW region and sample 2 with 40 repeats, were ready for device test. The *I-V* characteristic curves, spectral responsivity and current responsivity were measured to characterize the QWIP devices. *I-V* curves were swept under different temperature by Keithley 236. Figure 5 shows a set of *I-V* curves of our detectors at various temperatures from 40 K to 85 K. The desirable symmetry of the curves illustrates the good material quality and successful fabrication process. The *I-V* curves exhibited different appearance because of the variable period of QWs. The bias voltage in test is too high so that the barrier of QWs in sample 1 was broken down and the current increase dramatically. The same phenomenon was not observed for sample 2 since it has more repeat of wells in MQW region and the bias is not high enough.

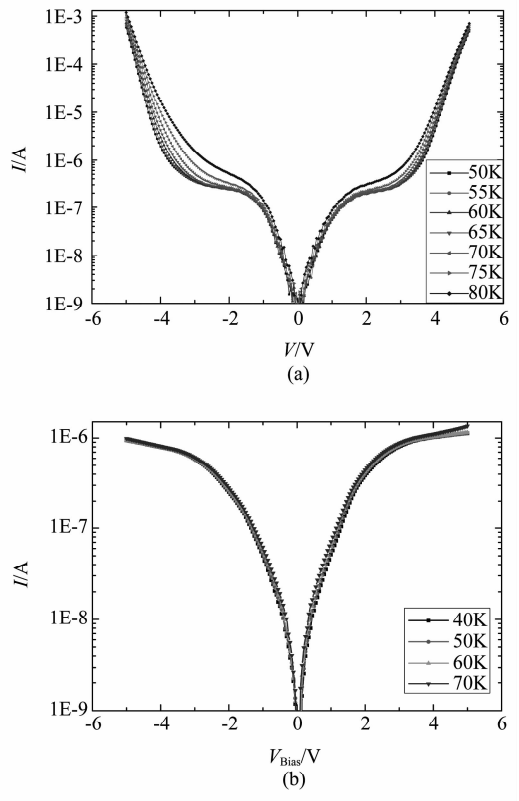

Fig. 5　*I-V* characteristic curves of QWIP device samples at different temperature. All curves exhibited favorable symmetry
图5　不同温度下两个量子阱器件样品的 *I-V* 曲线. 所有的样品曲线都表现出了良好的对称性

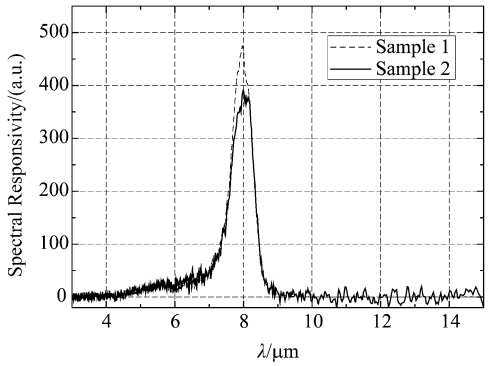

Fig. 6　Spectral responsivity curves at 50 K of the two device samples with 20 and 40 wells, respectively. The peaks of the responsivity curves are at 7.96 and 7.98 μm, excellently dovetailed with designed value
图6　两个量子阱周期分别为20 和40 的量子阱器件样品50 K 时的光谱响应. 峰值处于 7.96 和 7.98 μm 处,与设计值非常吻合

The spectral responsivity curve was measure by FTIR for both sample 1 and sample 2 at 50 K, which is shown in Fig. 6. The curve indicated that the peak absorption of our detectors occur at 7.96 μm for sample 1 and 7.98 μm for sample 2. While our designed peak detection wavelength is 8.0 μm, the experimental result was in excellent agreement with the theoretically expected value. Both high quality of material growth and device fabrication contribute to this result. This satisfactory accordance between theoretical result and experimental result proved that the modeling and calculation that we conducted was reasonable.

In addition we measured the black body detectivity for our sample detectors. A current responsivity of 0.13A/W and the peak detectivity is 8×10^{10} cmHz$^{1/2}$/W was measured for sample 2 under 4 V bias voltage.

4　Conclusions

In summary, we modeled GaAs/AlGaAs QWIP using one band effective mass approximation and envelop function approximation to, and we made use of shooting method in our calculation. In order to accurately find out the energy level in QWs which determine the peak wavelength, we included higher order effect of band nonparabolicity in our design. The structure parameters with an objective peak wavelength of 8 μm were calculated. Corresponding structure was grown by MBE and individual detectors with 20 and 40 QWs were fabricated. Measured *I-V* characteristic curves at different temperature exhibited very good symmetry, indicating the high quality of material and device. FTIR spectroscopy showed that the peak detection wavelengths of our two kinds of detectors were 7.96 and 7.98 μm, which is in very good accordance with theoretically calculated value.

Acknowledgements

The authors are very grateful to Professor Li Ning and Professor Li Zhi-feng, from National Key Laboratory of Infrared Physics, for the characterization of the detectors´performance. We also express our thanks to colleagues in Key Laboratory of Infrared Imaging Materials and Detectors for helpful discussion.

REFERENCES

[1] Levine B F, Malik R J, Walker J, *et al*. Strong 8.2 μm infrared intersubband absorption in doped GaAs/AlAs quan-

(下转第 496 页)

[4] Maestrini A, Ward J, Gill J, *et al*. A 1.7-1.9 THz local oscillator source[J]. *IEEE Microwave and Wireless Components Letters*, 2004, **14**(6): 253-255.
[5] Ward J, Schlecht E, Chattopadhyay G, *et al*. Capability of THz sources based on Schottky diode frequency multiplier chains[C]. *In* 2004 *IEEE MTT-S International Microwave Symposium Digest*. 2004. 3: 1587-1590.
[6] Maestrini A, Ward J S, Gill J J, *et al*. A 540-640-GHz high-efficiency four-anode frequency tripler [J]. *IEEE Transactions on Microwave Theory and Techniques*, 2005, **53**(9): 2835-2843.
[7] Porterfield D, Crowe T, Bishop W, *et al*. A high pulsed power frequency doubler to 190 GHz[C]. *In The Joint* 30*th International Conference on Infrared and Millimeter Waves and* 13*th International Conference on Terahertz Electronics*. 2005. 1: 78-79.
[8] Jeffrey L, Hesler W L B, Thomas W. Crowe multiplier development for the upper ALMA local oscillator bands[C]. *In* 17*th International Symposium on Space Terahertz Technology*. Paris. 2006: 215-218.
[9] Siles J V, Maestrini A, Alderman B, *et al*. A single-waveguide in-phase power-combined frequency doubler at 190 GHz[J]. *IEEE Microwave and Wireless Components Letters*, 2011, **21**(6): 332-334.
[10] Wang H, Rollin J-M, Alderman B, *et al*. Design of a low noise integrated sub-harmonic mixer at 183GHz using European Schottky diode technology[C]. *In* 4*th ESA Workshop On Millimetre Wave Technology and Applications*. Finland, 2006.
[11] Faber M T, Chramiec J, Adamski M E. Microwave and millimeterwave diode frequency multipliers[C]. Boston-London: Artech House, 1995: 104-107.
[12] Oswald J E , Siegel P H. The application of the FDTD method to millimeter-wave filter circuits including the design and analysis of a compact coplanar strip filter for THz frequencies [J]. *IEEE MTT-S International Microwave Symposium Digest*. 1994. **1**: 309-312.
[13] McMaster T F, Schneider M V, Snell W W. Millimeter-wave receivers with subharmonic pump[J]. *IEEE Transactions on Microwave Theory and Techniques*, 1976, **24**(12): 948-952.
[14] Kezai T, Sciuto R, Vorst AV. Experimental evidence of mounting grooves and serration patyerns on fin lines characteristics[J]. *International Journal of lnfrared and Millimeter Waves*. 1993, **14**: 1035-1046.
[15] Saini K S. A novel gallium arsenide-quart-based approach towards larger band-width Schottky diode frequency multipliers[D]: [Doctor Thesis]. Virginia: University of Virginia, 2003.
[16] Urzainqui I E. Electromagnetic band gap technology for millimetre wave applications[D]: [Doctor Thesis]. Pamplona: University Publica de Navarra, 2004.
[17] Porterfield D. A 200 GHz broadband, fixed-tuned, planar doubler[C]. *In Proceedings of the Tenth International Symposium on Space Terahertz Technology*. 1999: 463.
[18] [OL]. http://vadiodes.com/
[19] Zhang Y, LinY G. 185GHz solid-state circuits frequency doubler[J]. *Journal of University of Electronic Science and Technology of China*, 2010, **39**(2): 232-235.
[20] Zhang S, Zhang B, Fan Y. Design of a 114GHz-135GHz passive tripler[C]. *In* 2010 *International Symposium on Signals Systems and Electronics* (*ISSSE*). Nanjing. 2010, 1-3.
[21] Yao C. Reaearch on microwave and millimeter wave frequency mixing and multiplying techniques and their applications[D]: [Doctor Thesis]. Nanjing: Southeast University, 2010.

(上接485页)

tum well waveguides [J]. *Applied Physics Letters*, 1987, **50**(5): 273-275.
[2] Lu W, Li L, Zheng H L, *et al*. Development of an infrared detector: Quantum well infrared photodetector[J]. *Science in China Series G: Physics, Mechanics & Astronomy*, 2009, **52**(7): 969-977.
[3] Rogalski A. Quantum well photoconductors in infrared detector technology[J]. *Journal of Applied Physics*, 2003, **93**(8): 4355-4391.
[4] Rogalski A. Material considerations for third generation infrared photon detectors[J]. *Infrared Physics & Technology*, 2007, **50**(2-3): 240-252.
[5] Harrison P. *Quantum wells, wires, and dots: Theoretical and computational physics of semiconductor nanostructure* [M]. Second ed. John Wiley & Sons Hoboken, NJ, 2005.
[6] Jin J P, Lin C. Design of optimized Quantum well infrared photodetector's structure including higher order effects[J]. *Proc. of SPIE*, 2010, 7658: 76581U1-76581U6.
[7] Panda S, Panda B K, Fung S. Effect of conduction band nonparabolicity on the dark current in a quantum well infrared detector[J]. *J. Appl. Phys.* 2007, **101**(4): 043705.
[8] Hirayama Y, Smet J H, Peng L H, *et al*. Feasibility of 1.55 μm intersubband photonic devices using InGaAs/AlAs pseudomorphic quantum well structures[J]. *Japanese J. Applied Phys.*, 1994, **33**: 890-895.
[9] Liu H C. Quantum well infrared photodetectors: The basic design and new research directions[J]. *Chinese Journal Of Semiconductor*, 2001, **22**(5): 529-537.
[10] Schneider H, Liu H C. *Quantum well infrared photodetectors: Physics and applications*[M]. 1 ed. Springer, New York, 2007.
[11] Vurgaftman I, Meyer J R , Ram-Mohan L R. Band parameters for III-V compound semiconductors and their alloys [J]. *J. Appl. Phys.*, 2001, **89**(11): 5815-5875.